



CHORUS

This is the accepted manuscript made available via CHORUS. The article has been published as:

## Anomalous magnetic structure and spin dynamics in magnetoelectric $\text{LiFePO}_4$

Rasmus Toft-Petersen, Manfred Reehuis, Thomas B. S. Jensen, Niels H. Andersen, Jiying Li, Manh Duc Le, Mark Laver, Christof Niedermayer, Bastian Klemke, Kim Lefmann, and David Vaknin

Phys. Rev. B **92**, 024404 — Published 6 July 2015

DOI: [10.1103/PhysRevB.92.024404](https://doi.org/10.1103/PhysRevB.92.024404)

# Anomalous magnetic structure and spin dynamics in magneto-electric LiFePO<sub>4</sub>

Rasmus Toft-Petersen,<sup>1</sup> Manfred Reehuis,<sup>1</sup> Thomas B. S. Jensen,<sup>2</sup> Niels H. Andersen,<sup>2</sup> Jiying Li,<sup>3</sup> Manh Duc Le,<sup>1,4</sup> Mark Laver,<sup>2,5,6</sup> Christof Niedermayer,<sup>5</sup> Bastian Klemke,<sup>1</sup> Kim Lefmann,<sup>7</sup> and David Vaknin<sup>3</sup>

<sup>1</sup>*Helmholtz Zentrum Berlin für Materialien und Energie, D-14109 Berlin, Germany*

<sup>2</sup>*Department of Physics, Technical University of Denmark, DK-2800 Kgs. Lyngby, Denmark*

<sup>3</sup>*Ames Laboratory and Department of Physics and Astronomy, Iowa State University, Ames, Iowa 50011, USA*

<sup>4</sup>*Center for Correlated Electron Systems, Institute for Basic Science (IBS), Seoul 151-747, Korea*

<sup>5</sup>*Laboratory for Neutron Scattering and Imaging,*

*Paul Scherrer Institut, CH-5232 Villigen, Switzerland*

<sup>6</sup>*Department of Metallurgy and Materials, University of Birmingham, Birmingham B15 2TT, United Kingdom*

<sup>7</sup>*Nanoscience Center, Niels Bohr Institute, University of Copenhagen, DK-2100, Denmark*

(Dated: June 9, 2015)

We report significant details of the magnetic structure and spin dynamics of LiFePO<sub>4</sub> by single crystal neutron scattering. Our results confirm a previously reported co-linear rotation of the spins away from the principal  $b$  axis and determine that the rotation is towards the  $a$  axis. In addition, we find a significant spin canting component along  $c$ . The possible causes of these components are discussed and their significance for the magneto-electric (ME) effect is analyzed. Inelastic neutron scattering along the three principal directions reveal a highly anisotropic hard plane consistent with earlier susceptibility measurements. Using a spin Hamiltonian, we show that the spin-dimensionality is intermediate between XY- and Ising-like, with an easy  $b$  axis and hard  $c$  axis. It is shown that *both* next-nearest neighbour (NNN) exchange couplings in the  $bc$  plane are in competition with the strongest nearest neighbour (NN) coupling.

PACS numbers:

## I. INTRODUCTION

In the past decade, there has been a notable upswing in the investigation of multiferroic materials that simultaneously exhibit multiple ferroic order parameters.<sup>1,2</sup> The magneto-electric (ME) materials, where such co-existing order parameters couple ferroelectricity with magnetization, have also experienced a revival of interest due to the scientific challenges to unravel the coupling mechanism<sup>2,3</sup>, as well as for their potential applications.<sup>4</sup> The *lithium-ortho-phosphates* group LiMPO<sub>4</sub> ( $M = \text{Mn, Co, Fe or Ni}$ ) all exhibit a ME effect in their low-temperature antiferromagnetic (AFM) phases.<sup>5</sup> In addition, both LiMnPO<sub>4</sub><sup>6</sup> and especially LiFePO<sub>4</sub><sup>7</sup> have been proposed and used as materials for lithium battery cathodes, LiFePO<sub>4</sub> finding current commercial value.<sup>8</sup> Just recently, a graphene-modified LiFePO<sub>4</sub>-cathode has been shown to have a drastically increased specific capacity.<sup>9</sup>

The spin-orbit coupling is emerging as a significant ingredient of the ME coupling in general and in the lithium-ortho-phosphates in particular.<sup>10-12</sup> In fact, the relative strength of the ME-effect in these transition metal based compounds seems to scale with the effective total orbital contribution also affecting the single ion anisotropy and the effective  $g$  factor. For instance, LiMnPO<sub>4</sub>, where the magnetic Mn<sup>2+</sup> ion has  $L = 0$  by Hund's rules, has a very small but finite higher-order orbital contribution<sup>12</sup> ( $\Delta g/g \rightarrow 0$ ) and displays the weakest ME-effect among its counterparts.<sup>5</sup> By contrast, LiCoPO<sub>4</sub> ( $L = 3$ ) has very significant orbital contributions with  $\Delta g/g \approx 0.3$  and large single-ion anisotropy<sup>13,14</sup> and exhibits a 40 times stronger ME-

coupling than that of LiMnPO<sub>4</sub>.<sup>5,15,16</sup> Intermediate in coupling strength are LiFePO<sub>4</sub> and LiNiPO<sub>4</sub> ( $\Delta g/g \approx 0.1$ )<sup>10</sup>. The zero field magnetic structure of the 4 magnetic ions in LiNiPO<sub>4</sub> is predominantly polarized along  $c$  but also slightly canted along  $a$  due to the Dzyaloshinsky-Moriya (DM) interaction. It has been shown that the ME effect in LiNiPO<sub>4</sub> can be explained as resulting from enhanced spin-canting that is induced by applied magnetic field.<sup>10</sup> In LiCoPO<sub>4</sub> and LiFePO<sub>4</sub>, a similar microscopic ME-mechanism is impossible since the spin polarization is along the crystallographic  $b$  axis<sup>18,19</sup>, perpendicular to which the  $Pnma$  symmetry prevents spin-components along  $a$  and  $c$ . However, co-linear rotations of the magnetic moments away from the  $b$  axis have recently been found in both compounds.<sup>20,21</sup> Such rotations suggest that the crystal structure symmetry is most likely lower than orthorhombic  $Pnma$  at  $T_N$ . In addition, such a spin-rotation can produce ferrotoroidicity<sup>22</sup> as observed in LiCoPO<sub>4</sub>.<sup>23</sup> By similarity, ferrotoroidicity should also be present in LiFePO<sub>4</sub>, the sign of which depends on the rotation of the magnetic moments.<sup>24</sup> Here, we report on the exact polarization of this additional spin component and an observed zero field spin canting in LiFePO<sub>4</sub>. Although these additional spin components are minor, they are shown in this work to enable a magneto-electric response via the DM interaction.

Spin waves obtained by inelastic neutron scattering (INS) experiments have shown magnetic frustration due to competing exchange couplings in all known lithium orthophosphates.<sup>14,20,25,26</sup> For LiNiPO<sub>4</sub>, the magnetic frustration with local XY anisotropy promotes a rich phase diagram including an elliptical and canted spin

TABLE I: Crystal structure parameters of  $\text{LiFePO}_4$  obtained from refinement of single crystal diffraction data ( $\lambda = 0.89\text{\AA}$ ) collected at room temperature using the  $Pnma$  space group. The thermal parameters  $U_{ij}$  (given in  $100\text{\AA}^2$ ) are in the form  $\exp[-2\pi(U_{11}h^2a^{*2} + \dots + 2U_{13}hla^*c^*)]$ . For symmetry reasons, the values  $U_{12}$  and  $U_{23}$  of the atoms located at the Wyckoff position  $4c$  are equal to zero for the space group  $Pnma$ .

Atom	Site	$x$	$y$	$z$	$U_{11}$	$U_{22}$	$U_{33}$	$U_{12}$	$U_{13}$	$U_{23}$	Occ.
Li	$4a$	0	0	0	2.18(1)	1.79(1)	1.14(1)	0.00(1)	0.00(1)	-0.45(1)	1.011(22)
Fe	$4c$	0.28197(4)	1/4	0.97484(9)	0.49(2)	0.51(2)	0.67(2)	0	0.01(1)	0	1
P	$4c$	0.09483(7)	1/4	0.41813(15)	0.43(3)	0.50(3)	0.35(3)	0	0.01(1)	0	1
O1	$4c$	0.09697(7)	1/4	0.74224(15)	0.82(3)	0.92(3)	0.39(2)	0	0.04(2)	0	1.006(7)
O2	$4c$	0.45711(7)	1/4	0.20581(15)	0.51(3)	0.88(3)	0.65(3)	0	0.05(2)	0	1.007(6)
O3	$8d$	0.16568(5)	0.04642(9)	0.28465(11)	0.91(2)	0.67(2)	0.67(2)	0.25(1)	0.11(1)	0.07(1)	0.993(5)

$$a = 10.3377(10)\text{\AA}, b = 6.0112(10)\text{\AA}, c = 4.6950(10)\text{\AA} \quad V = 291.76(8)\text{\AA}^3$$

spiral state at low temperatures.<sup>10,16,27,28</sup> In  $\text{LiFePO}_4$ , previous INS measurements reported only one excitation branch<sup>20</sup> that suggested an isotropic hard plane using a spin Hamiltonian with an Ising-like anisotropy.<sup>20</sup> This is not entirely compatible with subsequent susceptibility measurements showing an anisotropic hard plane.<sup>29</sup> In addition, the spin wave model used for  $\text{LiFePO}_4$  in previous studies<sup>20</sup> assumed only one next-nearest neighbor (NNN) interaction along the  $c$  axis and one out-of-plane. Theoretical calculations<sup>30</sup> and experimental results indicate that five exchange parameters are non-negligible. The dispersion of the magnetic excitations along  $00L$  had not been measured yet in  $\text{LiFePO}_4$ , making a concise evaluation of the degree of frustration in the  $bc$  plane difficult. In the present work, we address these issues by elastic and inelastic neutron scattering to establish a more complete spin Hamiltonian for  $\text{LiFePO}_4$ .

## II. EXPERIMENTAL DETAILS

High-quality  $\text{LiFePO}_4$  single crystals were grown by the standard flux growth technique.<sup>50</sup> The experimental purity and stoichiometry was confirmed by laboratory x-ray powder diffraction. A 0.35 g crystal nearly spherical in shape was used in all neutron experiments. Diffraction measurements were performed on the RITA-II triple axis spectrometer at the SINQ, Paul Scherrer Institute, Switzerland - using a wavelength of  $\lambda = 4.04\text{\AA}$  and with the sample placed in an ILL orange cryostat. Diffraction data were collected on the 4-circle diffractometer E5 at the BER II reactor of the Helmholtz Zentrum Berlin (HZB). At 300 K, we collected a full dataset with  $\lambda = 0.89\text{\AA}$  using a copper monochromator and an Er-filter. For the magnetic reflections below  $T_N = 50\text{ K}$ , we collected data sets at 10 K and 100 K using a PG monochromator with  $\lambda = 2.38\text{\AA}$  and a PG filter. For the low temperature measurements, we used a closed-cycle cryostat with a base temperature of 10 K. For a refinement of the crystal and magnetic structures, the program FullProf (Ref. 33) was used with nuclear scattering lengths  $b(\text{Li}) = -1.90\text{ fm}$ ,  $b(\text{O}) = 5.805\text{ fm}$ ,

$b(\text{P}) = 5.13\text{ fm}$ , and  $b(\text{Fe}) = 9.54\text{ fm}$ .<sup>34</sup> The magnetic form factor of the  $\text{Fe}^{2+}$  ion were taken from Ref. 35. In order to determine the absolute value of the magnetic moments we have refined the overall scale factor and extinction parameter from crystal structure refinements using the data collected at 300 K, well above the Néel temperature  $T_N = 47(3)\text{ K}$ . With the absorption and extinction corrected magnetic structure factors, we were able to obtain the magnetic moments of the iron atoms in the magnetically ordered state.

The INS measurements were performed on the newly upgraded FLEXX spectrometer at the HZB<sup>36</sup> (constant final energy with  $\lambda_f = 4.05\text{\AA}$ ). All the inelastic measurements were performed at 1.7 K using a standard ILL orange cryostat.

For heat capacity measurements, we used a 6.5 mg  $\text{LiFePO}_4$  single crystal of the same batch as the one used for neutron scattering. The measurements were done in zero field, using a Physical Property Measurement System (PPMS, Quantum Design) at the Laboratory for Magnetic Measurements, HZB.

## III. RESULTS AND DISCUSSION

### A. Crystal structure

In earlier works, the crystal structure of  $\text{LiFePO}_4$  was described in the orthorhombic space group  $Pnma$  (No. 62).<sup>31,32</sup> This space group symmetry could be confirmed from our analysis of the data set collected at room temperature. The Li and O3 atoms are located at the Wyckoff positions  $4a(0,0,0)$  and  $8c(x,y,z)$ , while all the other atoms Fe, P, O1, and O2 are located at the position  $4c(x,1/4,z)$ . A full data set of 3095 reflections (820 unique) was collected at 300 K using neutron wavelength  $\lambda = 0.89\text{\AA}$ . The refinements of a total of 41 parameters (the overall scale and extinction factor  $g$ , 11 positional, and 28 anisotropic thermal parameters) resulted in a residual  $R_F = 0.039$  (defined as  $R_F = \sum ||F_{\text{obs}}| - |F_{\text{calc}}|| / \sum |F_{\text{obs}}|$ ). For the secondary extinc-

TABLE II: Irreducible representations of the  $Pnma$  space group generated for the Wyckoff position  $4c$ .

$Pnma$	$\Gamma_1$	$\Gamma_2$	$\Gamma_3$	$\Gamma_4$	$\Gamma_5$	$\Gamma_6$	$\Gamma_7$	$\Gamma_8$
$x$	–	$F_x$	–	$G_x$	$C_x$	–	$A_x$	–
$y$	$G_y$	–	$F_y$	–	–	$A_y$	–	$C_y$
$z$	–	$G_z$	–	$F_z$	$A_z$	–	$C_z$	–

tion parameter  $g$ , which is related to a Gaussian mosaic distribution, we obtained the value  $g = 921(32) \text{ rad}^{-1}$ , resulting in a maximum extinction of 54 % (in  $F$ ) for the strongest Bragg reflection. The  $g$  value reveals a peak shape with a full width at half maximum (FWHM) of 2.48 minutes of arc. In the final refinement, we also have the occupancies of the Li and O atoms as free parameters. In Table I, where the results of the refinements are summarized, it can be seen that the atomic positions of both the Li and O atoms are fully occupied.

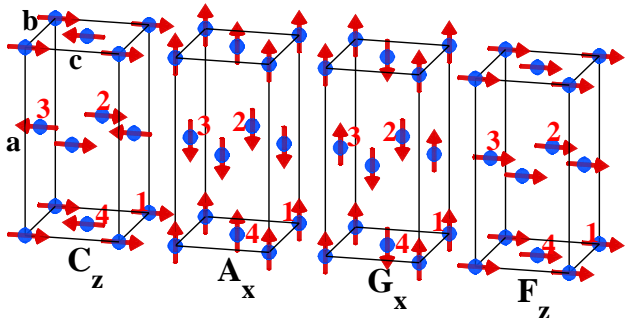


FIG. 1: (Color online) Irreducible basis vectors of  $\text{LiFePO}_4$  using the  $Pnma$  space group. Only the sub-lattice of magnetic ions is shown.

## B. Magnetic structure

Possible magnetic structures of the sublattice in  $\text{LiFePO}_4$  were deduced from representation analysis using the orthorhombic space group  $Pnma$  and the propagation vector  $\mathbf{k} = 0$ .<sup>37,38</sup> The four magnetic  $\text{Fe}^{2+}$  ions are located on the Wyckoff position  $4c$ :  $\mathbf{r}_1 = (1/4 + x, 1/4, -z)$ ,  $\mathbf{r}_2 = (3/4 + x, 1/4, 1/2 + z)$ ,  $\mathbf{r}_3 = (3/4 - x, 3/4, z)$  and  $\mathbf{r}_4 = (1/4 - x, 3/4, 1/2 - z)$ , where  $x = 0.03$  and  $z = 0.025$  in the orthorhombic unit cell. We have used the notation given in Refs. 10 and 27, denoting the four irreducible basis vectors  $A(+ - - +)$ ,  $G(+ - + -)$ ,  $C(+ + - -)$  and  $F(+ + + +)$ , where the brackets show the relative phase factors of the spins on the sites  $(\mathbf{r}_1, \mathbf{r}_2, \mathbf{r}_3, \mathbf{r}_4)$ . The 8 irreducible representations of the  $Pnma$  space group are given in Table II and examples of each symmetry class are shown in Fig. 1.

The intensity of magnetic Bragg scattering at any given point in reciprocal space is proportional to the magnetic

TABLE III: Squared structure factors ( $F^2$ ) and polarization factors ( $P^2$ ) for the main peaks reflecting the three observed components of the magnetic structure.

$hkl$	$F_C^2$	$F_A^2$	$F_G^2$	$F_F^2$	$P_x^2$	$P_y^2$	$P_z^2$	$I_{corr}$
012	14	0	2	0	1	0.86	0.14	5.3
001	0.5	0	15.5	0	1	1	0	0.46
100	0	15.4	0.6	0	0	1	1	0.0043
010	16	0	0	0	1	0	1	0.0044

neutron scattering cross-section which is proportional to  $|F_R(\mathbf{Q})|^2 |P(\mathbf{Q})|^2$  for a collinear structural component, where the structure factor ( $F$ ) and polarization ( $P$ ) factors are given by

$$F_R(\mathbf{Q}) = \sum_d \mathbf{m}_d^R e^{i\mathbf{Q}\cdot\mathbf{r}_d}; \quad \mathbf{P}(\mathbf{Q}) = \hat{\mathbf{Q}} \times (\hat{\mathbf{e}} \times \hat{\mathbf{Q}}). \quad (1)$$

Here  $\mathbf{m}_d^R$  is the magnetic moment of the ion at site  $d = 1, \dots, 4$  in the irreducible basis vector  $R = C, A, G, F$ ,  $\hat{\mathbf{Q}}$  is the unit vector along the neutron momentum transfer and  $\hat{\mathbf{e}}$  is the unit vector along  $\mathbf{m}_d^R$ . Table III lists  $|F_R(\mathbf{Q})|^2$  (normalized to unit magnetic moment) and  $|P(\mathbf{Q})|^2$  for  $R$  and all spin directions  $\hat{\mathbf{e}}$  parallel to  $x, y$  or  $z$  for 4 fundamental magnetic Bragg peaks, for which the temperature-dependence (using the E5 4-circle diffractometer) is presented below. The numbers in Table III represent the sensitivity of each peak to the different magnetic structures.

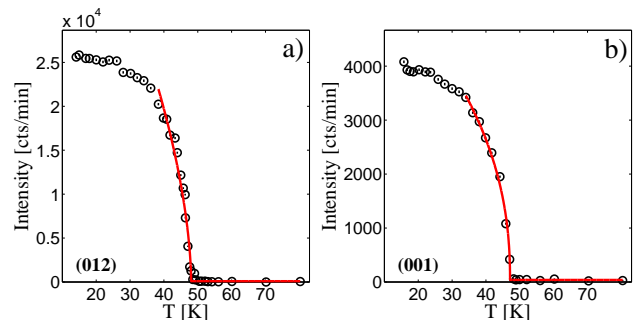


FIG. 2: (Color online) Temperature dependence of the two magnetic peaks 012 (a) and 001 (b). The red line represents a power law fit as a guide to the eye.

In agreement with Rousse et al.<sup>37</sup> strong magnetic intensities were found for the 101 and 210 reflections confirming the dominant  $C$ -type structure component along the  $y$ -direction. This ordering corresponds to the representation  $\Gamma_8 = [0, C_y, 0]$  given in Table II. For this magnetic structure, some magnetic reflections overlap with allowed nuclear peaks. The refinements of the crystal structure (above  $T_N$ ) shows a pronounced extinction effect, which manifests itself by a substantial reduction of

the strongest observed  $F^2$  values as compared to the calculated values. Therefore, the very strong 101 and 210 peaks have been left out of the final refinement. For tracking the order parameter, we monitored the structurally forbidden 001 and 012 magnetic reflections as a function of temperature (Fig. 2). The fit to the intensity versus temperature using a power law yields a Néel temperature of  $T_N = 47.0(1)$  K. This is smaller than previously reported values<sup>18,20</sup> but is most likely due to a temperature gradient in our cryostat setup, since  $T_N = 50.0(1)$  K was measured using the same sample in the RITA-II experiment, where the presence of exchange-gas reduces such temperature gradients. Due to the presence of strong extinction and the presence of a significant temperature gradient in the sample mount, the critical exponent is not subject to interpretation in this work. The overall scale factor and the extinction parameter were taken from the crystal structure refinement at 300 K, and were fixed for the refinement of the magnetic structure. In fact, for the reflections 001 and 012, we could obtain a satisfactory agreement between the observed and calculated  $F^2$  values resulting in a residual  $R(F^2) = 0.049$ . The refined magnetic moment  $\mu_y = 4.09(4)\mu_B$  ( $C_y$  component) is in good agreement with the moment value  $\mu_y = 4.19(5)\mu_B$  obtained earlier from neutron powder data.<sup>37</sup> Interestingly, the magnetic reflection 001 could

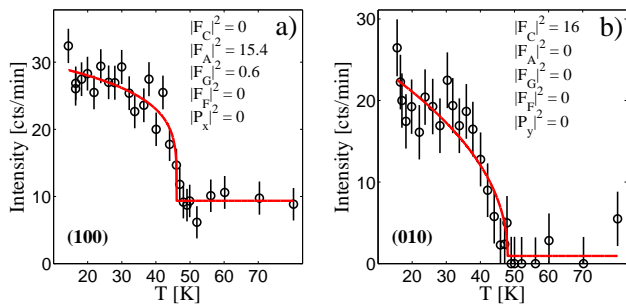


FIG. 3: (Color online) The intensity of the 100 peak reflecting the  $A_z$  component (a) and the 010 peak reflecting the  $C_x$  component. The integrated intensities of the magnetic scattering have similar values. The red line represents a power law fit as a guide to the eye.

not be observed in the neutron powder pattern reported by Rouse et al.<sup>37</sup>, but in the present single crystal work, this reflection is quite strong as shown in Fig. 2. In fact, a simulation of a powder pattern using the  $C$ -type ordering could not generate significant intensity at the position of the 001 reflection. Thus, it is clearly evident that single-crystal diffraction reveals more structural details than neutron powder diffraction. As a consequence, the pronounced extinction leads to a significant decrease of the strong magnetic reflection 012 leading to a much reduced ratio  $F^2(012)/F^2(001)$  in comparison to the powder data.

Fig. 3 shows the temperature dependence of the 100 and 010 integrated intensities as a function of temperature with a transition temperature in agreement with  $T_N$ . Both the 100 and the 010 peaks are not allowed by the  $C$ -type structure with a magnetic moment along the  $b$  axis, namely  $C_y$ . In Refs 20 and 21, magnetic intensity was found in the 010 reflection in  $\text{LiFePO}_4$  and  $\text{LiCoPO}_4$  respectively. This was interpreted in terms of a co-linear rotation of the spins away from the high symmetry  $b$  axis. These experiments were conducted on a triple axis spectrometer and confined to one scattering plane, and therefore without completely establishing the direction of the rotation or the detailed magnetic structure since this was the only deviant peak reported. The 010 reflection solely reflects  $C_x$  and  $C_z$  structure components due to the structure- and polarization factors. Here, we find weak magnetic intensity in the 010 reflection, but also in the 100 peak mainly reflecting  $A_z$  and  $A_y$  components (see Fig. 3). Since the intensities of the two deviant magnetic peaks are similar, and since  $C_x$  and  $A_z$  belong to the same irreducible representation, the simplest interpretation is that the structure is described by the vector  $[C_x, C_y, A_z]$ , which expressed in terms of irreducible representations is  $\Gamma_5 \oplus \Gamma_8$ . Thus, the magnetic structure has two deviant features, a co-linear rotation of the spins toward the  $a$  axis *and* a spin canting along the  $c$  axis. The refined spin rotation and canting moments are  $\mu_x = 0.067(5)\mu_B$  and  $\mu_z = 0.063(5)\mu_B$  along  $a$  and  $c$  respectively, corresponding to an overall rotation of the ordered moments of  $1.3(1)^\circ$  off the  $b$  axis (see Fig. 4).

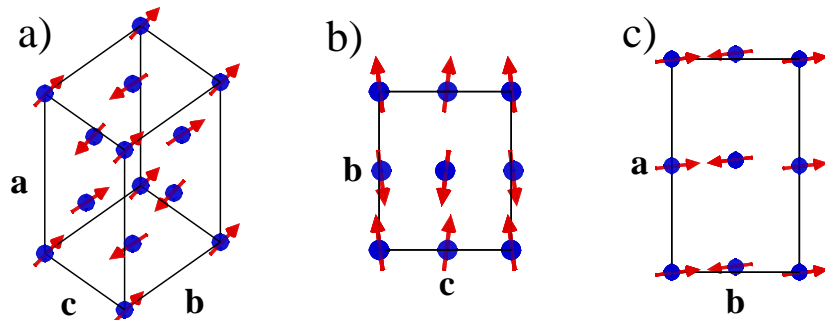


FIG. 4: (Color online) The magnetic structure of  $\text{LiFePO}_4$  (a), and the projections onto the  $bc$  plane (b) and  $ab$ -plane (c) respectively. The canting and rotation angles have been exaggerated for clarity.

### C. Crystal symmetry

The additional magnetic structure components in  $\text{LiFePO}_4$  have a non-trivial origin. Any term in the Hamiltonian quadratic in spin which would couple the main  $C_y$  structure to *any* of the canting components ( $A_i$  or  $G_i$ ) cannot be invariant with respect to all of the  $Pnma$  symmetries describing the *crystal structure* of  $\text{LiFePO}_4$ . This is due to the fact that the irreducible basis vector describing the main magnetic structure,  $C_y$ , is the only basis vector in its irreducible representation,  $\Gamma_8$ . It is interesting to note that a DM term of the form  $\mathcal{H}_{DM} = S_1^z S_4^x - S_1^x S_4^z + S_3^z S_2^x - S_3^x S_2^z$  is allowed by  $Pnma$  symmetry<sup>10</sup> and couples  $A_z$  with  $C_x$  components to make them energetically favourable. But even the existence of such a term in  $\text{LiFePO}_4$  cannot, within the Landau theory of second order phase transitions, lift the requirement that only order parameters belonging to a single irreducible representation can become critical at each transition. The observation in this work of order parameters from two irreducible representation implies that either another second order phase transition is present, or that the ordering transition is first order. From the data presented here it is obvious that all three structure components (i.e. the magnetic peaks 010, 100 and 012) represent conventional second order phase transitions with the same ordering temperature. The most probable cause of the observed magnetic structure in  $\text{LiFePO}_4$  is therefore that the structure is not  $Pnma$  at  $T_N$ . As an additional examination of whether a structural transition takes place below 300 K, we have measured the heat capacity of a 6.5 mg  $\text{LiFePO}_4$  single crystal. It is evident that the antiferromagnetic ordering transition is the only one below 300 K as shown in Fig. 5.

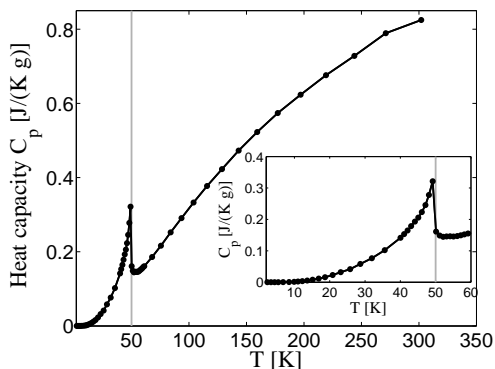


FIG. 5: The heat capacity of  $\text{LiFePO}_4$  vs. temperature at zero magnetic field. The magnetic phase transition is clearly evident at 50 K, and no sign of a structural phase transition is evident between 50-300 K. The statistical error are smaller than the marker size, but there can be a systematic error of up to 5 % in the  $C_p$  measurements.

Therefore, if the crystal structure has a lower symmetry than  $Pnma$  at all temperatures the deviation must be small enough not to be readily observed in this study as well as the many previous room temperature x-ray and neutron powder experiments.<sup>18,37,39,40</sup> There was no anomaly in the thermal variation of the strongest nuclear peaks between 10 and 100 K. These peaks have pronounced extinction, and a structural phase transition could cause a change in the degree of extinction, which could result in a strong change in intensity as observed earlier for  $\text{YVO}_3$  in Ref. 41, where the crystal structure changes from orthorhombic to monoclinic. It is possible that there is a small structural distortion, inherent and thus present at all temperatures. The corresponding lowering of the structural symmetry could result in  $C_y$ ,  $C_x$  and  $A_z$  belonging to the same irreducible representation and hence the same order parameter. This could also allow large enough DM or anisotropic exchange terms to generate the observed magnetic structure. Such a strong impact of minor structural details on the magnetic interactions (and hence the magnetic structure) are naturally very relevant for a microscopic explanation of the ME-effect. These structural details could be resolved in high resolution synchrotron X-ray experiments.

### D. Implications for the magneto-electric effect

The existence and strength of DM-terms depend entirely on the symmetry of the crystal lattice and the significance of the spin-orbit coupling, respectively<sup>45</sup>. In crystal fields of low symmetry like in  $\text{LiFePO}_4$ , the spin orbit coupling can restore some orbital momentum to the otherwise quenched ground state and produce large anisotropies in the  $g$ -tensor as reported for  $\text{LiFePO}_4$  in Refs 46 and 29. This orbital contribution to the magnetization can produce ME effects even in the absence of spin canting. In Ref. 11, it was calculated *ab initio* that the polar distortions created by an applied electrical field can cause an ME response in  $\text{LiFePO}_4$  by virtue of orbital magnetization. However, another route to a ME response is possible via the magnetic interactions *between* the  $\text{Fe}^{2+}$  ions. If the magnetic ground state contains a significant orbital contribution, a change in the crystal structure creating an electric polarization can have a strong impact on the DM-terms, and vice versa. Thus, lowering the crystal symmetry by allowing for an electric polarization the magnetic energy can be minimized via the DM-terms, as the field-induced change in spin canting changes the DM-energy of the system. For fields applied along the spins in a co-linear anti-ferromagnet, the DM-energy is unchanged since all spins are either parallel or anti-parallel. However, the observation of the anomalous  $A_z$  and  $C_x$  components makes both a superexchange- and DM-mediated mechanism for the ME-effect possible.

### 1. Field applied along $b$

In Ref. 10 a mechanism for the ME-effect for  $\text{LiNiPO}_4$  was proposed, facilitated by the asymmetry in the canting angles of spin pairs (1, 2) and (3, 4), induced by the applied field. This causes a difference in the super-exchange energy between the two spin pairs leading to the ME-effect. In  $\text{LiFePO}_4$ , due to the observed spin canting, a similar term is possible via the DM interaction for fields applied along  $b$ , where a similar asymmetry in canting angle occurs as shown in Fig. 6. For this purpose, the relevant DM-interaction allowed by  $Pnma$  symmetry is

$$\mathcal{H}_{DM} = D_{12}^y(S_1^z S_2^x - S_1^x S_2^z) + D_{34}^y(S_3^z S_4^x - S_3^x S_4^z) \quad (2)$$

where  $Pnma$  requires  $D_{12}^y = D_{34}^y$ . The observed minor structural components  $A_z$  and  $C_x$  of equal magnitude are minimized by such a term. The magnitudes of these components correspond to an overall rotation of all spins by  $\theta_c = 1.3^\circ$  away from the  $b$  axis.

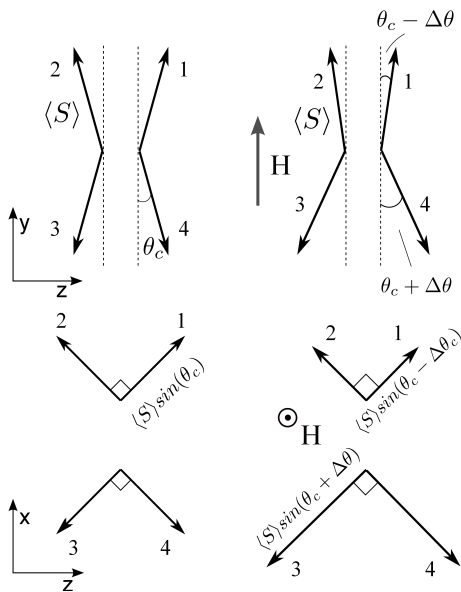


FIG. 6: The magnetic structure in fields applied along  $b$ . The small field-induced difference in canting angle between the two spin pairs (1,2) and (3,4) is evident. This corresponds to a difference in the magnitude of the  $A_z$  and  $C_x$  components in the  $ac$  plane.

For small fields along  $b$ , the system accommodates the Zeeman term by aligning spins (1, 2) along the field and rotate spins (3, 4) away from the  $b$  axis as shown on Fig. 6, with no change in anisotropy energy for small angles. The components in the  $ac$ -plane of spins 1 (3) and 2 (4) are perpendicular and have magnitude proportional to  $\langle S \rangle \sin(\theta_c \pm \Delta\theta) \approx \langle S \rangle (\theta_c \pm \Delta\theta)$  for small angles. Here  $\Delta\theta$  is the angular deviation from  $\theta_c$  in applied fields. The field-induced change in DM energy described by Eq. 2 can be written as:

$$\begin{aligned} \Delta E_{DM}^{P||x} &= \langle S \rangle^2 (D_{12}^y + D_{34}^y) \Delta\theta^2 \\ &+ 2 \langle S \rangle^2 (D_{34}^y - D_{12}^y) \theta_c \Delta\theta \end{aligned} \quad (3)$$

Eq. 3 can be minimized by a change in the DM interactions. Such changes can occur naturally by displacing the  $\text{PO}_4$  tetrahedra between the Fe ions, thereby changing the exchange paths and lowering the symmetry of the crystal lattice. If such a displacement along  $x$  allows changes in the DM-interactions that minimizes Eq. 3, the field induced canted structure can induce a ME-response. By applying a field along  $b$ , the Zeeman term removes the  $Pnma$  symmetry elements transforming  $S_y \rightarrow -S_y$  from the spin Hamiltonian. A polarization  $P_x$  removes the symmetry elements that transforms  $x \rightarrow -x$ . In Ref. 13 it was shown that removing these exact symmetry elements from the Hamiltonian lifts the requirement  $D_{12}^y = D_{34}^y$ , while any DM components  $D_{ij}^x$  or  $D_{ij}^z$  are still forbidden. From Eq. 3 it can be seen that via a change of the DM-components  $D_{12}^y \rightarrow D_{12}^y + \delta$  and  $D_{34}^y \rightarrow D_{12}^y - \delta$ , the DM energy is lowered by  $-4\delta \langle S \rangle^2 \theta_c \Delta\theta$ . Assuming that the change in DM-coupling is linear in displacement,  $\delta = \lambda_{DM}^x x$ , the energy difference is  $\Delta E_{DM}^{P_x} = -4 \langle S \rangle^2 \lambda_{DM}^x \theta_c \Delta\theta x$ . Such a displacement is resisted by the elastic forces in the lattice. The total energy difference of the displacement is then  $-4 \langle S \rangle^2 \lambda_{DM}^x \theta_c \Delta\theta x + kx^2$ , where  $k$  is the elastic constant for  $\text{PO}_4$  tetrahedron displacement. This expression has a minimum at  $x = 2k^{-1} \langle S \rangle^2 \lambda_{DM}^x \theta_c \Delta\theta$ . Assuming the same value of the ordered moment for all four spins,  $\Delta\theta \propto \chi_b H_y$  and the polarization is proportional to the displacement  $x$ , this change in the DM-terms gives a linear ME response  $P_x \propto 2k^{-1} \langle S \rangle^2 \lambda_{DM}^x \theta_c \chi_b H_y$ . This results in a ME coefficient  $\alpha_{xy}^{DM} \propto 2k^{-1} \langle S \rangle^2 \lambda_{DM}^x \theta_c \chi_b$ , similar to those described for other compounds in Refs. 47 10 and 48.

### 2. Field applied along $a$

For fields applied along  $a$ , a ME-effect can be mediated by the DM-interaction independent of the canting component  $A_z$ . The applied field induces a ferromagnetic component along  $x$ , canting spin pairs (1, 3) and (2, 4), or (1, 4) and (2, 3) as shown in Fig. 7. The Zeeman term removes symmetry elements transforming  $S_x \rightarrow -S_x$  while an electrical polarization along  $y$  removes the symmetry elements transforming  $y \rightarrow -y$ . This allows a DM-term of the form  $D_{ij}^z$ :<sup>13</sup>

$$\mathcal{H}_{DM} = D_{13}^z(S_1^y S_3^x - S_1^x S_3^y) + D_{24}^z(S_2^y S_4^x - S_2^x S_4^y). \quad (4)$$

Thus, in the small angle approximation the change in DM-energy is

$$\Delta E_{DM}^{P||y} = \langle S \rangle^2 (\delta D_{13}^z + \delta D_{24}^z) \Delta\theta, \quad (5)$$

where  $\delta D_{13}^z$  and  $\delta D_{24}^z$  are changes in the DM-terms upon polarization. Similar argument hold for DM-terms of the form  $D_{14}^z$  and  $D_{23}^z$ . If displacing the  $\text{PO}_4$  tetrahedra along  $y$  would cause such non-zero DM-terms  $\delta D_{13}^z = \delta D_{24}^z = \lambda_{DM}^y y$ , the change in DM energy of

such a displacement is  $-2\langle S \rangle^2 \lambda_{DM}^y \Delta\theta$ . Using similar arguments as for fields along  $b$ , the ME response would be  $x = k^{-1} \langle S \rangle^2 \lambda_{DM}^y \chi_a H_x$  and  $\alpha_{yx}^{DM} \propto k^{-1} \langle S \rangle^2 \lambda_{DM}^y \chi_a$ .

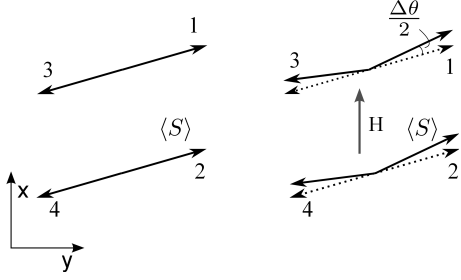


FIG. 7: Magnetic structure in fields along  $a$ . The induced ferromagnetic component along  $a$  creates a spin canting in the  $ab$  plane

### 3. Comparison with experiment

In this model, the ME-coefficients are proportional to  $\langle S \rangle^2 \chi$  for fields applied along both  $a$  and  $c$ . The temperature dependencies of  $\alpha_{xy}$  and  $\alpha_{yx}$  in  $\text{LiFePO}_4$  was measured in Ref. 5. A straightforward comparison of the DM-induced  $\alpha_{ij}(T)$  response to experiment can be made by calculating the temperature dependencies of the ME-coefficients directly from the experimental values of  $\langle S \rangle^2(T)$  and  $\chi(T)$ . We have used the the temperature dependency of the intensity of the weak 001 magnetic peak, as measured on RITA-II, as a credible measure of  $\langle S \rangle^2(T)$ . The susceptibilities  $\chi(T)$  for fields along  $a$  and  $b$  are taken from Ref. 42 and multiplied a proportionality factor  $d\Delta\theta/dM$  calculated from figure 6 and 7 assuming the same moment  $\langle S \rangle^2$  for all 4 ions. We use a scaling parameter  $C_i \propto \lambda_i^{DM}/k$  for both  $\alpha_{xy}$  and  $\alpha_{yx}$  to fit the low temperature response and these are the only free parameters used. The scaling parameters are similar with  $C_x/C_y = 0.55$  and the results are shown in Fig. 8.

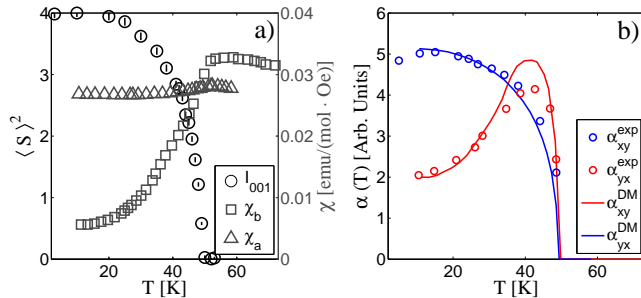


FIG. 8: (Color online) a) The scaled intensity of the 001 peak measured on RITA-II and the molar susceptibilities for fields along  $a$  and  $b$  from Ref. 42. b) The measured ME-coefficients  $\alpha_{xy}$  and  $\alpha_{yx}$  taken from Ref. 5 compared to the calculated temperature dependency in arbitrary units.

The temperature dependencies of  $\alpha_{xy}$  and  $\alpha_{yx}$  are in good agreement with experiment at low and intermediate temperatures. The high temperature maximum of  $\alpha_{xy}$  is slightly below the expected value. This might be due to non-identical moment lengths at higher temperatures; a larger moment on spins 1 and 2 compared to spins 3 and 4 would reduce the asymmetry in the DM-energy and hence reduce the ME-response. The model gives the correct peak temperature of  $\alpha_{xy}$ , which is an improvement over the model presented in Ref. 5. The close agreement of the  $\alpha_{yx}$  temperature dependency shows the significance of  $\langle S \rangle^2$  for the strength of the ME-coupling, which might be of interest for future ab initio calculations.

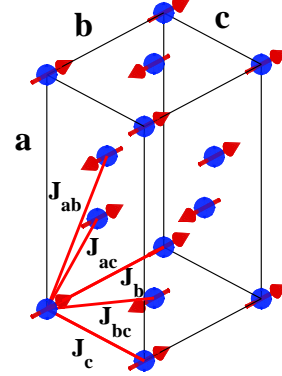


FIG. 9: (Color online) The magnetic unit cell and spin structure with the exchange couplings used in this work to analyze the spin dynamics.

### E. Spin dynamics

The spin excitations measured in this work have been analyzed using a similar model as for the spin waves in  $\text{LiNiPO}_4$ <sup>26,47</sup>,  $\text{LiMnPO}_4$ <sup>25</sup> and  $\text{LiCoPO}_4$ .<sup>14</sup> Three exchange parameters in the strongly coupled  $bc$  plane have been used, one nearest neighbor (NN)  $J_{bc}$  (Fe-O-Fe) and two next-nearest-neighbours (NNN),  $J_b$  and  $J_c$  (Fe-O-O-Fe) and two out-of-plane interactions (Fe-O-P-O-Fe)  $J_{ac}$  and  $J_{ab}$ . These interactions are depicted on the magnetic unit cell in Fig. 9. We use two parameters to describe the single ion anisotropy,  $D_a$  and  $D_c$ , allowing for an anisotropic hard plane while the anisotropy term for the easy  $b$  axis is fixed to  $D_b = 0$ . This is a modification of the model used in Ref. 20, where only one NNN interaction, one out-of-plane interaction and one single ion anisotropy parameter was used (thus,  $D_a = D_c$ ,  $J_{ac} = J_{ab}$  and  $J_c = J_b$  in terms of our model). Here we assume that the spin canting is too small to lift degeneracies in the spin excitation spectrum, justified by the small value of the canting angle and the observation of only two excitation branches. We therefore neglect weak interactions such as the DM- and anisotropic exchange-interactions



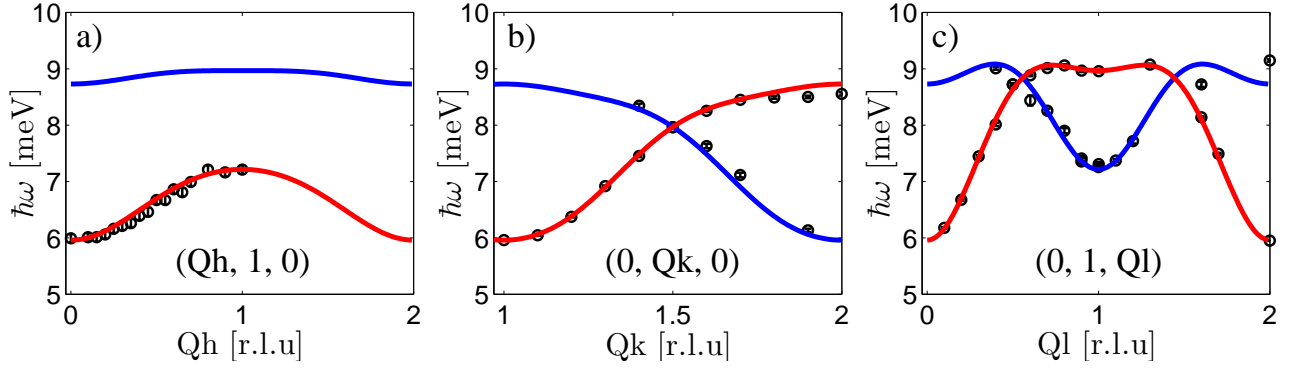


FIG. 10: (Color online) The magnetic excitations of LiFePO<sub>4</sub>. a) Measurement of the dispersion of the low-energy branch along  $Qh$  taken from Ref. 20. b-c) The data from this work, where both branches are observed. Two model dispersion branches were fitted to the data - a high intensity one (red) and a low intensity one (blue).

(as done in Ref. 10). The following Hamiltonian is used:

$$\mathcal{H} = \frac{1}{2} \sum_{ij} J_{ij} \mathbf{S}_i \cdot \mathbf{S}_j + \sum_{\alpha,i} D_{\alpha} S_{\alpha i}^2 \quad (6)$$

To calculate the spin wave dispersion we apply Holstein-Primakoff linear spin wave theory,<sup>26,49</sup> assuming the ground state magnetic structure to be purely  $C_y$  (see Fig. 9). The eigenenergies of the magnetic Hamiltonian are

$$\hbar\omega = \sqrt{A^2 - (B \pm C)^2}, \quad (7)$$

where

$$A = 4S(J_{bc} + J_{ab}) - 2S\{J_b[1 - \cos(\mathbf{Q} \cdot \mathbf{r}_5)] + J_c[1 - \cos(\mathbf{Q} \cdot \mathbf{r}_6)] + J_{ac}[2 - \cos(\mathbf{Q} \cdot \mathbf{r}_7) - \cos(\mathbf{Q} \cdot \mathbf{r}_8)]\} + (S - 1/2)(D_a + D_c) \quad (8)$$

$$B = (S + 1/2)(D_a - D_c) \quad (9)$$

$$C = 2J_{bc}S[\cos(\mathbf{Q} \cdot \mathbf{r}_1) + \cos(\mathbf{Q} \cdot \mathbf{r}_2)] + 2J_{ab}S[\cos(\mathbf{Q} \cdot \mathbf{r}_3) + \cos(\mathbf{Q} \cdot \mathbf{r}_4)], \quad (10)$$

and  $\mathbf{r}_{1,2} = \frac{1}{2}(\mathbf{b} \pm \mathbf{c})$ ,  $\mathbf{r}_{3,4} = \frac{1}{2}(\mathbf{a} \pm \mathbf{b})$ ,  $\mathbf{r}_5 = \mathbf{b}$ ,  $\mathbf{r}_6 = \mathbf{c}$  and  $\mathbf{r}_{7,8} = \frac{1}{2}(\mathbf{a} \pm \mathbf{c})$ . It is evident from Eq. (3) that when  $D_a \neq D_c$ ,  $\hbar\omega$  becomes multivalued and two excitation branches should be seen. This is exactly what is observed, as shown Fig 11 a) and b), where two well separated excitations reveal pronounced anisotropy in the hard plane.

Fig. 10 shows the dispersion curves of these two observed spin wave branches along the three principal directions (the data along  $Qh$  is taken from Ref. 20). Using Eq. (7) we refined by non-linear least square fit the exchange parameters and the single-ion-anisotropies simultaneously from the branches in all three principal directions. The solid lines in Fig. 10 are calculations using Eq. (7) with the parameters that are listed in Table IV. All exchange terms are AFM in nature. From the

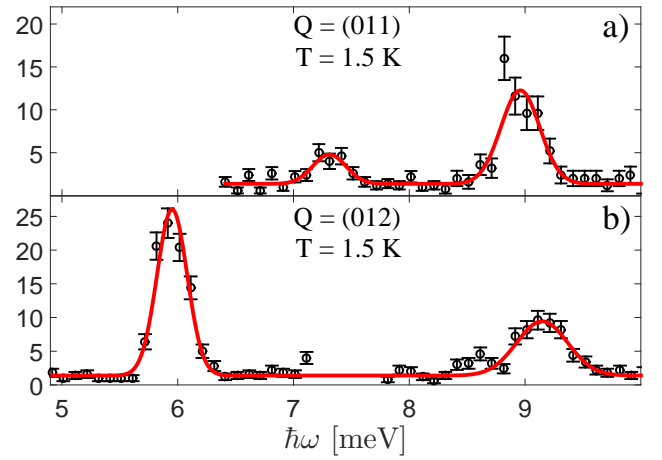


FIG. 11: (Color online) a-b) Energy scans at  $Q = (011)$  and  $Q = (012)$  respectively - two distinct branches are evident in both scans. The red lines are fits to double Gaussian distributions.

strengths of the single ion anisotropies compared with the exchange terms, it is clear that the system is described by a model intermediate between Ising and XY. There is a hard axis along  $c$  and intermediate magnetic anisotropy axis  $a$  along which the anisotropy term is weaker than the exchange field but still significant. The quasi-2D nature of LiFePO<sub>4</sub> is less pronounced ( $J_{bc}/J_{ab} \approx 5$ ) than in LiNiPO<sub>4</sub> ( $J_{bc}/J_{ab} \approx 10$ ).

All three interactions in the strongly coupled  $bc$  plane are antiferromagnetic (AFM) leading to magnetic frustration. Evidently,  $J_{bc}$  and  $J_{ab}$  are strong enough to generate the observed commensurate structure of ferromagnetic  $ac$  planes alternating along  $b$ . Using a simple model for such layers<sup>51</sup>, with a nearest-layer coupling of  $J_1$  and a next-nearest-layer coupling  $J_2$  one can evaluate whether an incommensurate structure modulated perpendicular to the planes (in this case  $b$ ) is energetically favourable. The criterion for spontaneous IC order is  $|J_1| < 4J_2$ . Using the effective parameters

TABLE IV: The magnetic exchange interactions of LiFePO<sub>4</sub> in meV.

$J_{bc}$	$J_b$	$J_c$	$J_{ab}$	$J_{ac}$	$D_a$	$D_c$
0.77(7)	0.30(6)	0.14(4)	0.14(2)	0.05(2)	0.62(12)	1.56(3)

for LiFePO<sub>4</sub>,  $J_1 = 2J_{bc} + 2J_{ab} = 1.76(20)$ meV and  $4J_2 = 4J_b = 1.14(23)$ meV, it is evident that the exchange interactions in LiFePO<sub>4</sub> fall short of causing spontaneous IC magnetic order. This is not the case in LiNiPO<sub>4</sub> where  $J_1 = 2.7(2)$  meV and  $4J_2 = 2.68(4)$  meV.<sup>26</sup> This causes the Ni-system to be on the verge between C and IC order, and in fact both order parameters are observed at different temperatures.<sup>10</sup> Contrary to LiNiPO<sub>4</sub>, LiFePO<sub>4</sub> has a non-negligible  $J_c$  coupling, so that not only the  $J_b$  term but also the  $J_c$  and  $J_{ac}$  terms are in competition with the stronger  $J_{bc}$  and  $J_{ab}$  terms. This introduces another element of magnetic frustration *within* the ferromagnetic planes, as shown in figure 12. Whether or not there are field-induced magnetic phase transitions in LiFePO<sub>4</sub> as in LiNiPO<sub>4</sub><sup>53</sup> and LiCoPO<sub>4</sub><sup>52</sup> remains to be seen.

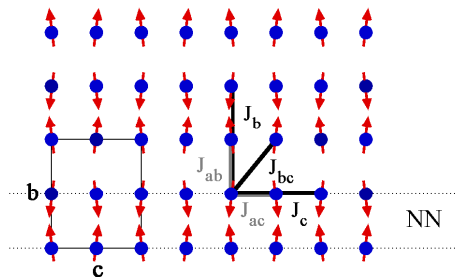


FIG. 12: (Color online) The structure of LiFePO<sub>4</sub> projected onto the  $bc$  plane, with the in-plane couplings shown in black, and the out-of-plane couplings shown in grey. The ferromagnetic  $ac$  planes are coupled to their nearest neighbours via  $J_{bc}$  and  $J_{ab}$ , in competition with the NNN couplings  $J_b$  and  $J_c$ .

## IV. CONCLUSION

We have determined the zero field magnetic structure of LiFePO<sub>4</sub> and found that the co-linear rotation of the spins is accompanied by a spin canting of the same magnitude - and thus two distinct irreducible representations are present. These findings strongly suggest that the crystal structure may have a lower symmetry than  $Pnma$  at  $T_N$ . This deviant spin structure permits an ME-effect mediated via the DM-interaction for fields along  $b$  that would otherwise be impossible. The spin waves along  $Qk$  and  $Ql$  have been thoroughly measured, and two distinct branches are found, indicative of a highly anisotropic hard plane. We have determined that there are three non-negligible competing interactions in the  $bc$  plane which introduces an element of frustration within the ferromagnetic planes that is not present in the other compounds of the family.

## Acknowledgments

Jens Jensen of the University of Copenhagen is greatly acknowledged for illuminating discussions. Work was supported by the Danish Agency for Science, Technology and Innovation under DANSCATT and by the Swiss NSF via contract PP002-102831. Research at Ames Laboratory is supported by the US Department of Energy, Office of Basic Energy Sciences, Division of Materials Sciences and Engineering under Contract No. DE-AC02-07CH11358. Neutron experiments were performed at the Helmholtz-Zentrum Berlin für Materialien und Energie, and at the SINQ neutron spallation source at the Paul Scherrer Institute, Switzerland. We thank HZB and PSI for the allocation of neutron radiation beam time.

- <sup>1</sup> W. Eerenstein, N. D. Mathur and J. F. Scott, *Nature* **442**, 759-765 (2006).
- <sup>2</sup> S. W. Cheong and M. Mostovoy, *Nature Materials* **6**, 13 (2007).
- <sup>3</sup> M. Kenzelmann et al., *Phys. Rev. Lett.* **95** 087206 (2005).
- <sup>4</sup> M. Bibes and A. Barthelemy, *Nature Materials* **7**, 425 (2008).
- <sup>5</sup> M. Mercier, Ph.D. thesis, Université de Grenoble (1969).
- <sup>6</sup> V. Aravindan, et. al., *J. Mater. Chem. A*, **1**, 3518-3539 (2013).
- <sup>7</sup> A. Yamada, S. C. Chung and K. Hinokuma, *J. Electrochem. Soc.* **148**, 3, A224-A229 (2001).
- <sup>8</sup> M. Dubarry, B. Y. Liaw, *Journal of Power Sources*, **194**, 1, 541-549 (2008).
- <sup>9</sup> L. Hu, et. al., *Nature Comm.* **4**, 1687 (2013).
- <sup>10</sup> T. B. S. Jensen, et. al., *Phys. Rev. B* **79**, 092412 (2009).
- <sup>11</sup> A. Scaramucci, et. al., *Phys. Rev. Lett.* **109**, 197203 (2012).
- <sup>12</sup> R. Toft-Petersen, et. al., *Phys. Rev. B* **85** 224415 (2012).
- <sup>13</sup> R. Toft-Petersen, Ph. D Thesis, Tech. Uni. Denmark (2012).
- <sup>14</sup> W. Tian, et al. *Phys. Rev. B*, **78**, 184429, (2008).
- <sup>15</sup> J. P. Rivera, *Ferroelectrics* **161**, Issue 1, (1994).
- <sup>16</sup> I. Kornev, et. al., *Phys. Rev. B*, **62** 12247 (2000).
- <sup>17</sup> A. Abragam and M. H. L. Pryce, *Proc. R. Soc. Lon. A*, 01/1951; 206(1085):173-191 (1951).
- <sup>18</sup> R. P. Santoro and R. E. Newnham, *Acta Cryst.* **22**, 344 (1967).
- <sup>19</sup> R. P. Santoro et. al., *J. Phys. Chem. Solids*. **27** 1192 (1966).
- <sup>20</sup> J. Li, et. al. *Phys. Rev. B*, **73** 024410 (2006).
- <sup>21</sup> D. Vaknin, et.al, *Phys. Rev. B*, **65**, 224414, (2002).
- <sup>22</sup> C. Ederer and N. Spaldin, *Phys. Rev. B* **76**, 214404 (2007).
- <sup>23</sup> B. van Aken, *Nature* **449**, 702-705 (2007).

- <sup>24</sup> A. S. Zimmermann et. al., *Eur. Phys. J. B* **71**, 355-360 (2009).
- <sup>25</sup> J. Li, et al, *Phys. Rev. B*, **79**, 144410, (2009).
- <sup>26</sup> T. B. S. Jensen, et al., *Phys. Rev. B* **79**, 092413 (2009).
- <sup>27</sup> R. Toft-Petersen, et al., *Phys. Rev. B*. **84** 054408 (2011).
- <sup>28</sup> D. Vaknin, et. al., *Phys. Rev. Lett.* **92**, 207201 (2004).
- <sup>29</sup> G. Liang, et. al., *Phys. Rev. B*, **77**, 064414, (2008).
- <sup>30</sup> D. Dai, et. al., *Inorg. Chem.*, 2005, 44 (7), pp 2407 (2005).
- <sup>31</sup> S. Geller and J. L. Easson, *Acta Crystallogr.* **18**, 258 (1960).
- <sup>32</sup> P. S. Herle, B. Ellis, N. Coombs, and A.F. Nazar, *Nat. Mater.* **3**, 147 (2004).
- <sup>33</sup> J. Rodriguez-Carvajal, FullProf: a Program for Rietveld Refinement and Pattern Matching Analysis, Abstract of the Sattelite Meeting on Powder Diffraction of the XV Congress of the IUCr, p. 127, Toulouse, 1990.
- <sup>34</sup> V. F. Sears, in: *International Tables of Crystallography*, vol. C, ed. A. J. C. Wilson (Kluwer, Dordrecht, 1992) p. 383.
- <sup>35</sup> P. J. Brown, in: *International Tables of Crystallography*, vol. C, ed. A. J. C. Wilson (Kluwer, Dordrecht, 1992) p. 391.
- <sup>36</sup> M. D. Le, et. al., *Nucl. Instr. and Methods A*, **729**, 220-226 (2013).
- <sup>37</sup> G. Rousse, et. al., *Chem. Mater.* 15, 4082 (2003).
- <sup>38</sup> E. F. Bertaut, *Acta Cryst. A* 24, 217 (1968); see also J. de Phys. Coll. C1 32(2-3) 462 (1971) and *J. Magn. Magn. Mater.* 24, 267 (1981).
- <sup>39</sup> A. S Andersson, et. al. *Solid State Ionics*, **130** 1-2, 41-52 (2000).
- <sup>40</sup> Z. Chen, et. al. , *J. Mater. Chem.*,**21**, 5604 (2011).
- <sup>41</sup> M. Reehuis, et. al, *Phys Rev. B*, **73** 094440 (2006).
- <sup>42</sup> D. P. Chen, et. al., *J. Appl. Phys.* **101**, 09N512 (2007).
- <sup>43</sup> Rossat-Mignod, *J. Methods of experimental physics* (Academic Press Inc, 1987) Vol. 23, part C, chapter 19.
- <sup>44</sup> J. Rodriguez-Carvajal, *Physica B* **192**, 55-69 (1993).
- <sup>45</sup> Toru Moriya, *Phys. Rev.* **120**, 91 (1960).
- <sup>46</sup> J.G. Creer, G. J. Troup, *Physics Letters A* **32**, 6, 439440 (1970).
- <sup>47</sup> T. B. S. Jensen, Ph. D Thesis, Tech. Uni. Denmark (2008).
- <sup>48</sup> Rado, et. al., *Phys. Rev. Lett.* **6** 609 (1961).
- <sup>49</sup> P. A. Lindgaard, et. al., *Chem. Solids* **28**, 1357 (1967).
- <sup>50</sup> V. I. Fomin, et. al., *Low Temp. Phys.*, 28, 203 (2002).
- <sup>51</sup> T. Nagamiya, in *Solid State Physics*, edited by F. Seitz and D. Turnbull Academic, New York, 1967, Vol. 29, p. 346
- <sup>52</sup> N. F. Kharchenko, et. al., *Low Temp. Phys.* 36, 558 (2010);
- <sup>53</sup> V. M. Khrustalyov, et. al. *Czech. Journal of Physics* **54**, 4, pp 27-30 (2004)